Supplemental material for:

NMR study of $Ni_{50+x}Ti_{50-x}$ Strain-Glass

Rui Li, Jacob Santiago, Daniel Salas, Ibrahim Karaman, and Joseph H. Ross Jr.

1) X-ray measurements

Further x-ray diffraction (XRD) details are as follows:

a) Results for $x = 0.1$ sample: For the $x = 0.1$ sample with the conventional martensite phase transition, the cubic B2 lattice constant refined to 3.0205 Å at 400 K. Aside from 0.8% per mole formula-unit Ti_2Ni, no TiC or other phases were detected [1]. For 100 K, fig S1(a) shows the refinement described in the text fitted to the B19′ structure [2] combined with the small Ti_2Ni reflections. The structure given in reference [3] gave nearly identical results once the atomic parameters were relaxed. The small fitted lattice constant changes for 100 K relative to the reported low temperature values [2] are consistent with the reported anisotropic thermal expansion of the B19′ phase [4]. The broad intensity peak near 12° in the difference curve has no features that could be matched to a known phase, although the position corresponds to the region of largest intensity for the R phase. Assuming this possibility, an added R phase component [5] led to a refined value of 8% phase fraction, but only with the addition of very large microstrain broadening corresponding to 4.5% RMS strain for the R phase. This improved the R_w from 15.9% to 12.5% [Fig. S1(b)]. A similar fit was obtained assuming heavily size broadened R phase (refined to 7 nm domain size), and a nearly equivalent fit could be obtained with a heavily broadened orthorhombic B19 phase [6], making it unclear what might be the significance of this feature.

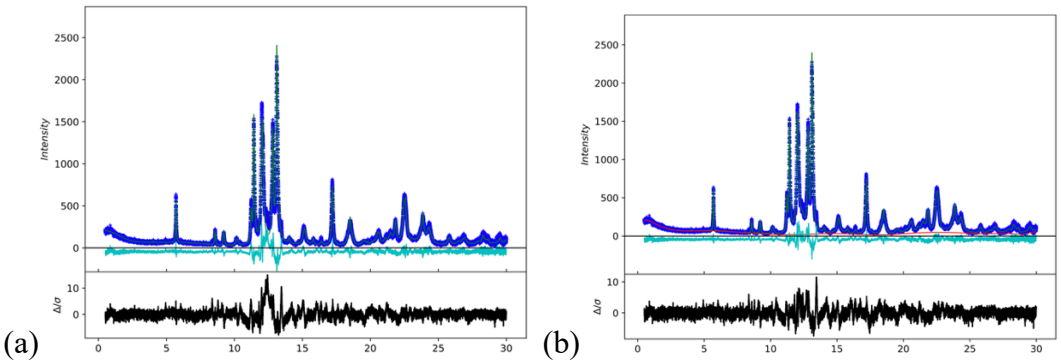

Figure S1: XRD refinement results for $x = 0.1$ ($Ni_{50.1}Ti_{49.9}$) sample at 100 K. (a) B19′ phase [2] plus 0.8 % Ti_2Ni. Refined lattice constants $a = 2.8804$ Å, $b = 4.1152$ Å, $c = 4.6543$ Å, $\beta = 97.58°$. (b) with heavily strain-broadened R phase as described in text.

b) Results for $x = 1.2$ and 2.0 strain glass samples: For the strain glass samples, as described in the main text, all spectra were fitted to a model having reflections associated with a microstrain-broadened B2 phase overlaying an identical B2 phase with narrow reflection profiles. Results for 200 K and 295 K are shown in Fig. S2, while the 100 K results are shown in the main text. For $x = 1.2$, refinement yielded 26% phase fraction for the broadened B2 phase, with 1.6% microstrain

at 295 K increasing to 2.2% at 100 K. For x = 2.0 the results yielded 1.9% microstrain/48% phase fraction changing to 1.9%/41% at 100 K.

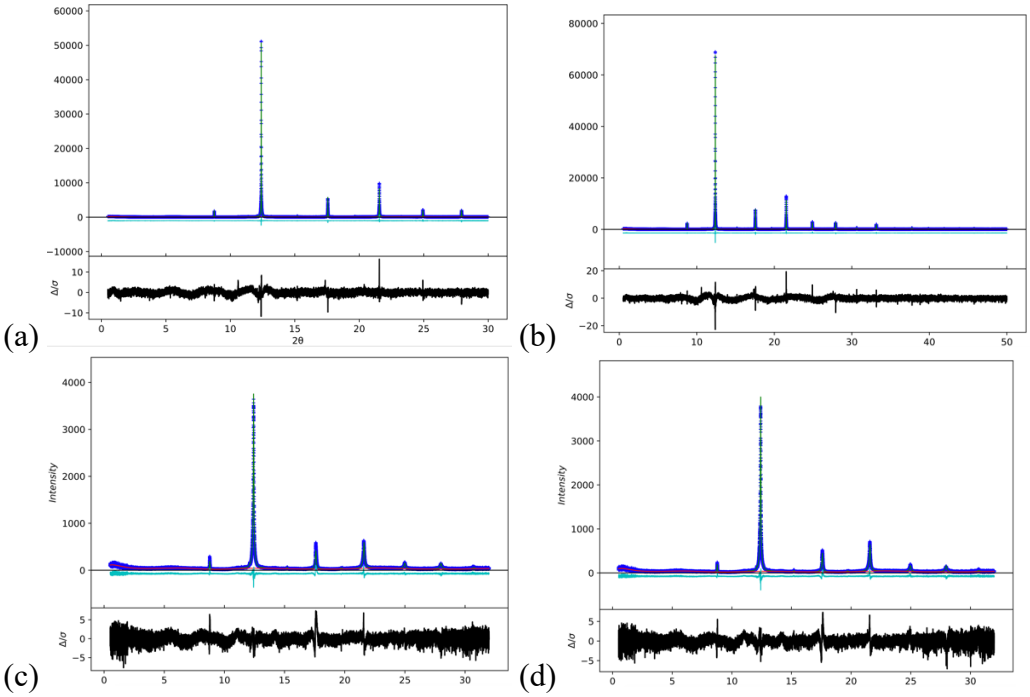

Figure S2: Refined $Ni_{50.1}Ti_{50-x}$ XRD results for (a) x = 1.2 at 200 K (R_w = 8.6%); (b) x = 1.2 at 295 K (R_w = 9.7%); (c) x = 2.0 at 200 K (R_w = 14.3%); (d) x = 2.0 at 295 K (R_w = 14.1%).

A further comparison is shown in Fig. S3, for which R phase [5], with 10% phase fraction per mole formula unit and the same peak profile as the B2 phase, has been added to the refined curves for T = 100 K. It is clear that the R phase is not represented in the data, as compared to the reported results [7] after a prolonged soaking time.

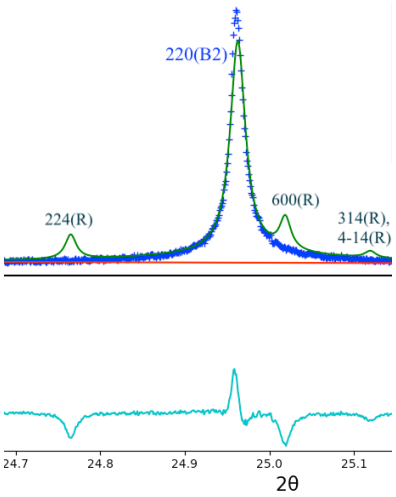

Figure S3: XRD refinement for x = 1.2 sample at 100 K, fitted to B2 phase with added R phase (10% R-phase fraction) added to the calculated curves. Results shown in the vicinity of the (220) B2 reflection, with individual calculated reflections labeled.

The fitted B2-phase lattice constants for the $Ni_{50+x}Ti_{50-x}$ strain glass materials are shown in Fig. S4. The results obtained at 200 and 295 K correspond to a linear coefficient of thermal expansion $\beta = 11$ and 9.1×10^{-6}/K for x = 1.2 and 2.0 respectively. These can be compared to values in the range $12 - 13 \times 10^{-6}$/K measured for the B2 phase in equiatomic NiTi at higher temperatures [8–10]. Extending to lower temperatures, one can expect a somewhat nonlinear behavior according to the thermodynamic equality $\beta = \frac{\gamma C_V}{9B}$ [11,12], where C_V is the specific heat and B is the bulk modulus, with the Grüneisen constant γ taking into account the lattice anharmonicity. Taking the calculated [13] B = 150 GPa for the B2 phase, and with the Debye temperature taken to be $\Theta_D = 290$ K [14], we obtained the curves $a = a(0)[1 + \int \beta \, dT]$ shown in the figure. These are based on a Debye function for C_V, assuming B and γ to be temperature independent. The least-squares fit gives $a(0)$ = 3.0025 (2.9967) Å for x = 1.2 (2.0), and corresponding Grüneisen constants γ = 1.6 (1.35). These estimated values for γ are in line with typical values for metals, and though there may be some composition dependence for B and Θ_D, there is no indication that the results depart from typical thermal-expansion behavior, even though the strain-glass freezing temperatures fall in the middle of the range. Thus similar to the xrd profiles described above, which exhibit very little change going into the strain glass phase, the lattice constants also display no obvious signs of anomalous behavior when sampled across the spin glass freezing temperature.

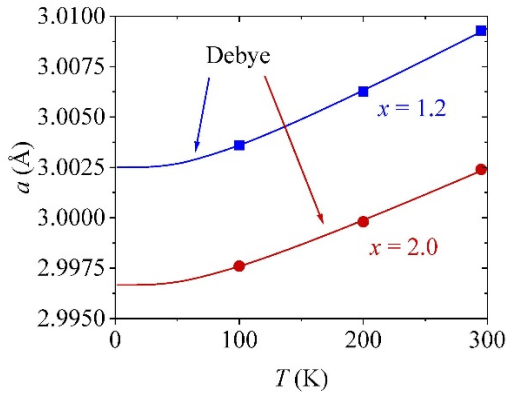

Figure S4: Lattice constants for B2 phase obtained from XRD refinements for $Ni_{50.1}Ti_{50-x}$ strain glass samples x = 1.2 and x = 2.0, along with Debye-model thermal expansion curves described in the text.

2) DFT calculations: Electric Field Gradients and Korringa T_1

DFT calculations were performed using the Wien2k package, with more details given in the main text. Partial densities of states are shown in Figures S5 and S6 for the NiTi B19′, B2, and R phases, and Fermi-level parameters are given in Table S1.

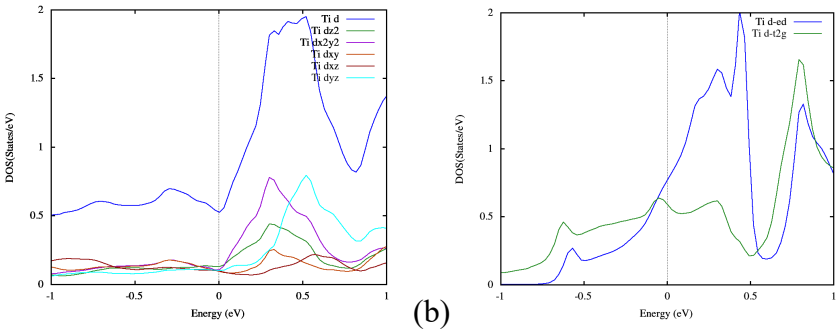

(a) (b)

Figure S5: Ti partial densities of states near the Fermi energy for NiTi in (a) B19' structure with structural parameters from [3]. Blue curve: total Ti-$g_d(E)$. Other curves: $g_d(E)$ for individual d orbitals as shown. (b) B2 structure with a = 3.015 Å. Blue: e_g symmetry; Green: t_{2g} symmetry.

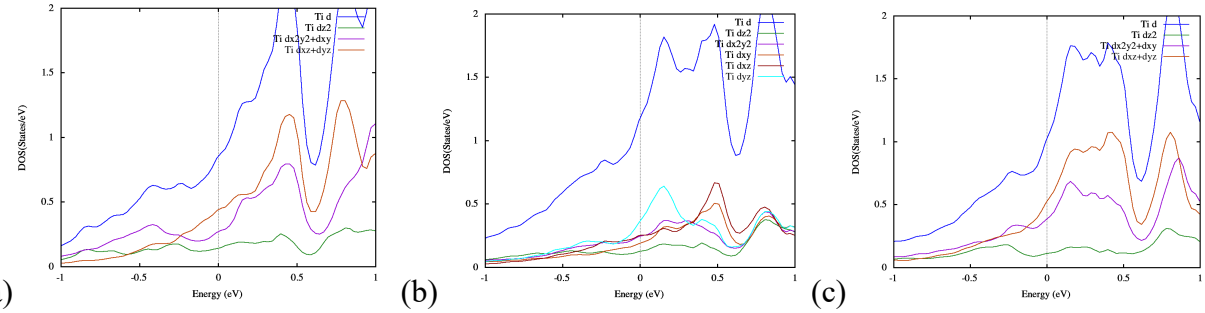

(a) (b) (c)

Figure S6: Ti partial densities of states near the Fermi energy for NiTi R-phase, parameters from [5]: (a) site 1; (b) site 2; (c) site 3. Blue curves: total Ti-$g_d(E)$. Other curves for orbitals indicated.

For Korringa-type spin-lattice relaxation in NMR, as given in the main text, a general expression is,

$$\frac{1}{T_1T} = 4\pi\hbar\gamma_n^2 k_B g_d^2(E_F) \sum_i (H_i^{HF})^2 F_i, \qquad [S1]$$

where *i* refers to individual hyperfine terms, with orbital (*orb*), core polarization (*CP*), and dipolar (*dip*) relevant here and H_i^{HF} is the hyperfine field. Also γ_n is the nuclear gyromagnetic ratio, $g_d(E_F)$ is the Ti-site local *d*-electron Fermi level density of states. Expressions for the numerical factors F_i are given for general symmetry in [15], depending on the mixture of *d* orbitals at E_F. Since both H_{orb}^{HF} and H_{dip}^{HF} are equal to $\frac{\mu_0}{4\pi} 2\mu_B \langle r^{-3} \rangle$, we report the orbital and dipolar F_i values together in the table. For core polarization, $F_{CP} = \lambda_{z^2}^2 + \lambda_{x^2-y^2}^2 + \lambda_{xy}^2 + \lambda_{yz}^2 + \lambda_{xz}^2$, with λ_j representing the fraction of $g_d(E_F)$ due to the j^{th} orbital, so that $\sum \lambda_j = 1$. For all of the phases considered here, the Ti *d*-orbitals contribute in a relatively uniform way, so that F_{CP} is close to the minimum value of 0.2 in all cases (Table S1). Along with the larger H_{orb}^{HF} compared to H_{CP}^{HF}, the orbital contribution to $^1/_{T_1T}$ thus turns out to be significantly larger than the others. Taken together, these factors along with Equation [S1] yield the calculated Korringa $^1/_{T_1T}$ values shown in the table.

Table S1: Calculated local densities of states, Ti-site hyperfine parameters, and Ti-NMR Korringa-$1/(T_1T)$, and EFG parameters for NiTi structures as shown. Factors F_{orb}, F_{dip}, F_{CP} for orbital, dipolar, and core polarization hyperfine interactions are calculated using general relationships given in [15].

structure	multiplicity	$g_{total}(E_F)$ states/NiTi unit/eV	$g_d(E_F)$ d-states/Ti atom/eV	$F_{orb}+F_{dip}$	F_{CP}	calculated $1/(T_1T)$ [1/(sK)]	$^{47}\nu_Q$ [kHz]	η
B2 (a)	1	3.182	1.350	0.371	0.222	0.0215	0	–
B19' (b)	2	1.478	0.547	0.426	0.203	0.0037	1080	0.99
R (c):								
site 1	1		0.856	0.422	0.210	0.0090	1700	0
site 2	6		1.180	0.405	0.214	0.0165	–1100	0.96
site 3	2		1.024	0.409	0.215	0.0126	1620	0
site-weighted average		2.447	1.109			0.0148	1280	–

(a) Cubic B2 phase with a = 3.015 Å.
(b) B19' parameters from reference [3].
(c) R phase parameters from reference [5].

References:

[1] J. Mentz, J. Frenzel, M. F.-X. Wagner, K. Neuking, G. Eggeler, H. P. Buchkremer, and D. Stöver, Mater. Sci. Eng. A **491**, 270 (2008).

[2] W. Bührer, R. Gotthardt, A. Kulik, O. Mercier, and F. Staub, J. Phys. F: Met. Phys. **13**, L77 (1983).

[3] Y. Kudoh, M. Tokonami, S. Miyazaki, and K. Otsuka, Acta Metall. **33**, 2049 (1985).

[4] Z. Deng, Q. Li, Y. Onuki, and Q. Sun, J. Alloys Compd. **909**, 164682 (2022).

[5] H. Sitepu, Powder Diffr. **24**, 315 (2009).

[6] X. Huang, G. J. Ackland, and K. M. Rabe, Nat. Mater. **2**, 307 (2003).

[7] Y. Ji, D. Wang, X. Ding, K. Otsuka, and X. Ren, Phys. Rev. Lett. **114**, 055701 (2015).

[8] K. L. Fukami-Ushiro and D. C. Dunand, Metallurgical and Materials Transactions A **27**, 193 (1996).

[9] P. D. Bogdanoff and B. Fultz, Philos. Mag. B **81**, 299 (2001).

[10] S. Qiu, V. B. Krishnan, S. A. Padula, R. D. Noebe, D. W. Brown, B. Clausen, and R. Vaidyanathan, Appl. Phys. Lett. **95**, 141906 (2009).

[11] N. Ashcroft, and N. D. Mermin, Solid State Physics (Holt, Rinehart and Winston, 1976).

[12] B. Fultz, Prog. Mater. Sci. **55**, 247 (2010).

[13] F. Yu and Y. Liu, Computation **7**, 57 (2019).

[14] N. Singh, A. Talapatra, A. Junkaew, T. Duong, S. Gibbons, S. Li, H. Thawabi, E. Olivos, and R. Arróyave, Comput. Mater. Sci. 112, **347** (2016).

[15] B. Nowak, Solid State Nucl. Magn. Reson. **21**, 53 (2002).